Beam dynamics in high intensity cyclotrons including neighboring bunch effects: Model, implementation, and application

J. J. Yang (杨建俊),[1,2,3,*] A. Adelmann,[2,†] M. Humbel,[2] M. Seidel,[2] and T. J. Zhang (张天爵)[1]

[1]*China Institute of Atomic Energy, Beijing, 102413, China*
[2]*Paul Scherrer Institut, Villigen, CH-5234, Switzerland*
[3]*Department of Engineering Physics, Tsinghua University, Beijing, 100084, China*

(Received 16 March 2009; published 14 June 2010)

Space-charge effects, being one of the most significant collective effects, play an important role in high intensity cyclotrons. However, for cyclotrons with small turn separation, other existing effects are of equal importance. Interactions of radially neighboring bunches are also present, but their combined effects have not yet been investigated in any great detail. In this paper, a new particle in the cell-based self-consistent numerical simulation model is presented for the first time. The model covers neighboring bunch effects and is implemented in the three-dimensional object-oriented parallel code OPAL-CYCL, a flavor of the OPAL framework. We discuss this model together with its implementation and validation. Simulation results are presented from the PSI 590 MeV ring cyclotron in the context of the ongoing high intensity upgrade program, which aims to provide a beam power of 1.8 MW (CW) at the target destination.

DOI: 10.1103/PhysRevSTAB.13.064201 PACS numbers: 29.20.dg, 29.27.Bd, 41.20.Cv

I. INTRODUCTION

Since the invention of the classic cyclotron several decades ago, increasingly higher beam intensities are required to provide more powerful tools for many new scientific endeavors, such as spallation neutron sources and in the future accelerator driven systems that are foreseen to reduce nuclear waste. In high intensity cyclotrons, space-charge effects play an important role for the following reasons. First, with the absence of longitudinal focusing in cyclotrons, the longitudinal space-charge force causes additional acceleration for head particles and deceleration for tail particles, which may lead to an increase in energy spread. Second, there is a strong radial-longitudinal coupling which is influenced by nonlinear radial and longitudinal space-charge forces. Last, the space-charge force can reduce the vertical tune and increase the vertical beam size, which can cause beam losses when the vertical size extends beyond the aperture of the accelerator [1].

As shown in [2–7] and experimentally verified at the PSI injector II [8], an intense particle beam which is properly matched to a separate sector cyclotron develops a spatial stationary circular bunch distribution. Consequently, the halo is significantly reduced and a corresponding longitudinal decrease of the beam size is observed. We note that Kleeven gave in his thesis [9] an ''early'' hint on this remarkable effect and in [5] a compact derivation can be found. On a very practical side, because of the compact stationary distribution we can operate the 3rd harmonic resonator, the former flattop resonator in the PSI injector II, in acceleration mode.

Nonlinear space-charge effects in cyclotrons are complex because of the complicated magnetic topology (reference trajectory with nonconstant curvature). Typically there are two approaches to deal with this difficulty: one is an approximation with analytic and semianalytic models which are inexpensive to compute [5,9]. With such models we can obtain a qualitative understanding of the problem. In the past, a number of models have been developed based on this philosophy, such as the sector model, disk model, sphere model, and the so-called Needle model [3,4,10,11]. Another more accurate approach is numerical simulation with macroparticles. In this field, typically two different technologies have used to solve space-charge fields: particle-particle (P-P) methods [12] and particle-mesh (P-M) methods [6,7]. In P-P methods, the fields imposed on a given particle are obtained by directly summing up the contributions of all other particles at this position. Limited by its low computation efficiency $\mathcal{O}(n^2)$ with n denoting the number of simulation particles, it is impossible to utilize these methods when the number of particles is large (above 1×10^6), even on current state-of-the-art supercomputers. On the contrary, in P-M methods the fields are calculated on the discrete domains. Because of its high efficiency and high precision, P-M based particle-in-cell (PIC) methods [13] are widely used in parallel macroparticle simulation codes for different types of accelerators and beam lines [6,14–17] as well as many other areas of computational science, thanks to the development of parallel computation technology during recent years. The parallel PIC model is the method of choice in this study on the beam dynamics of high intensity cyclotrons.

For high intensity cyclotrons, single bunch space-charge effects are not the only contribution. Along with the steady increase of beam current, the mutual interaction of neighboring bunches in radial direction becomes more and more

*yangjianjun2000@tsinghua.org.cn
†andreas.adelmann@psi.ch

important, especially at large radii where the distances between neighboring bunches diminishes, and even the overlap can occur. One example is the PSI 590 MeV ring cyclotron [18] with a production current of 2 mA in CW operation and a beam power on target of approximately 1.2 MW. An ambitious upgrade program for the PSI ring cyclotron is in progress, aimed for 1.8 MW CW beam power on target. The concept involves replacing four aluminum cavities by new copper cavities with peak voltages increasing from about 0.7 MV to above 0.9 MV, meanwhile the old flattop cavity remains in use with peak voltage standing at 11.2% of the main voltage. After the planned upgrade is finished, the total turn number can be significantly reduced, e.g., from more than 220 turns to less than 170 turns.

The turn separation is consequently increased as shown in Fig. 1, but remains at the same order of magnitude as the measured radial bunch size (at the 1σ level) and is also dependent on the increasing bunch current. Therefore, when the beam current increases from 2 to 3 mA, the correct treatment of space-charge effects is of great importance. This includes the mutual space-charge effects between radially neighboring bunches.

Another example is the 100 MeV compact cyclotron (CYCIAE-100) under construction at CIAE [19]. Although its beam current is only 200 to 500 μA, because of the small energy gain per turn (about 200 keV), the turn separation is far more smaller than the beam size at outer radii (at the extraction, $\Delta R = 1.5$ mm) and multiple bunches will overlap.

Because of the complexity of the problem, it is impossible to evaluate neighboring bunch effects precisely and self-consistently by explicit analytic expressions. However, high performance computation makes it possible to treat this problem in greater detail. To our knowledge, little research has been undertaken in neighboring bunch effects, and the only published work in that regard was by Pozdeyev [7]. He introduced "rigid auxiliary bunches" in his serial code CYCO which uses the azimuthal angle as the independent variable.

In Sec. II, a new PIC based self-consistent numerical simulation model is presented which, for the first time, covers neighboring bunch effects. Section III describes our three-dimensional object-oriented parallel simulation code OPAL-CYCL, a flavor of the OPAL framework. The results of performance testing and code benchmarking are presented in Sec. IV, and followed by its applications on the PSI 590 MeV ring cyclotron in Sec. V. The last section is devoted to the conclusion of the paper.

II. BASIC EQUATIONS AND PHYSICAL MODEL

A. PIC model in cyclotron

In the cyclotrons and beam lines under consideration, the collision between particles can be neglected because the typical bunch densities are low. In time domain, the general equations of motion of charged particle in electromagnetic fields can be expressed by

$$\frac{d\mathbf{p}(t)}{dt} = q(c\boldsymbol{\beta} \times \mathbf{B} + \mathbf{E}), \tag{1}$$

where m_0, q, and γ are rest mass, charge, and the relativistic factor. With $\mathbf{p} = m_0 c\gamma\boldsymbol{\beta}$ we denote the momentum of a particle, c is the speed of light, and $\boldsymbol{\beta} = (\beta_x, \beta_y, \beta_z)$ is the normalized velocity vector. In general, the time (t) and position ($\mathbf{x}$) dependent electric and magnetic vector fields are written in abbreviated form as $\mathbf{B}$ and $\mathbf{E}$.

If $\mathbf{p}$ is normalized by $m_0 c$, Eq. (1) can be written in Cartesian coordinates as

$$\begin{aligned}
\frac{dp_x}{dt} &= \frac{q}{m_0 c}E_x + \frac{q}{\gamma m_0}(p_y B_z - p_z B_y),\\
\frac{dp_y}{dt} &= \frac{q}{m_0 c}E_y + \frac{q}{\gamma m_0}(p_z B_x - p_x B_z),\\
\frac{dp_z}{dt} &= \frac{q}{m_0 c}E_z + \frac{q}{\gamma m_0}(p_x B_y - p_y B_x).
\end{aligned} \tag{2}$$

The evolution of the beam's distribution function $f(\mathbf{x}, c\boldsymbol{\beta}, t)$ can be expressed by a collisionless Vlasov equation:

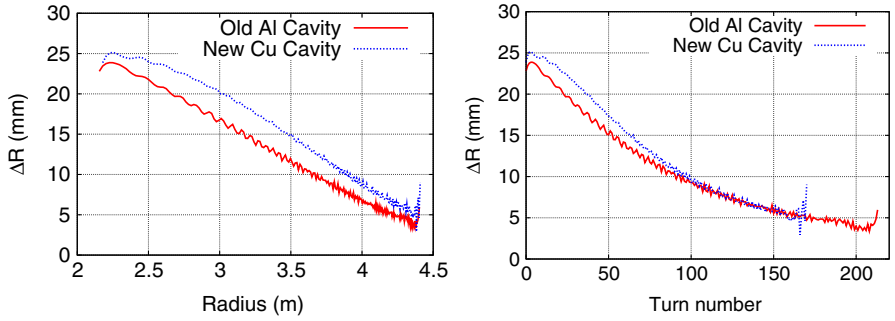

FIG. 1. (Color) Comparison of calculated turn separation for centroid particles before (red line) and after (blue line) upgrade of the PSI ring cyclotron. The main cavity voltage is set to 0.735 and 0.9 MV for aluminum and copper, respectively, while the flattop is set to 11.2% of the main voltage.

$$\frac{df}{dt} = \partial_t f + c\boldsymbol{\beta} \cdot \nabla_x f + q(\mathbf{E} + c\boldsymbol{\beta} \times \mathbf{B}) \cdot \nabla_{c\boldsymbol{\beta}} f = 0, \tag{3}$$

where $\mathbf{E}$ and $\mathbf{B}$ include both external applied fields, space-charge fields, and other collective effects such as wake-fields,

$$\mathbf{E} = \mathbf{E}_{\text{ext}} + \mathbf{E}_{\text{sc}}, \qquad \mathbf{B} = \mathbf{B}_{\text{ext}} + \mathbf{B}_{\text{sc}}. \tag{4}$$

In order to model a cyclotron, the external electromagnetic fields are given by measurement or by numerical calculations.

The space-charge fields can be obtained by a quasistatic approximation. In this approach, the relative motion of the particles is nonrelativistic in the beam rest frame, so the self-induced magnetic field is practically absent and the electric field can be computed by solving Poisson's equation,

$$\nabla^2 \phi(\mathbf{x}) = -\frac{\rho(\mathbf{x})}{\varepsilon_0}, \tag{5}$$

where ϕ and ρ are the electrostatic potential and the spatial charge density in the beam rest frame. The electric field can then be calculated by

$$\mathbf{E} = -\nabla\phi, \tag{6}$$

and back-transformed to yield both the electric and the magnetic fields, in the lab frame, required in Eq. (4) by means of a Lorentz transformation. Because of the large gap in our cyclotron, the contribution of image charges and currents are minor effects compared to space charges [1], and hence it is a good approximation to use open boundary conditions.

The combination of Eqs. (3) and (5) constitutes the Vlasov-Poisson system. In the content followed, the method of how to solve these equations in cyclotrons using PIC methods is described in detail.

Considering that particles propagate spirally outwards in cyclotrons, and the longitudinal orientation changes continuously, three right-handed Cartesian coordinate systems are defined, as shown in Fig. 2. The first coordinate system is the fixed laboratory frame $\mathbf{S}_{\text{lab}}$, in which the external field data is stored and the particles are tracked. Its origin is the center of the cyclotron and its X-Y plane is the median plane and the positive direction of Z axis points to the vertical direction.

The second coordinate system is the local instantaneous frame $\mathbf{S}_{\text{local}}$, which is a temporal auxiliary frame for the space-charge solver. Its origin O' is the mass center of the beam and the orientation of the Y' axis is coincident with the average longitudinal direction and the positive orientation of the Z' axis points to the vertical direction.

The third coordinate system is the beam rest frame $\mathbf{S}_{\text{beam}}$, which is comoving with the centroid of the beam. It has the same orientation and origin as $\mathbf{S}_{\text{local}}$, but the length in longitudinal direction is scaled by $1/\gamma$ due to relativistic effects.

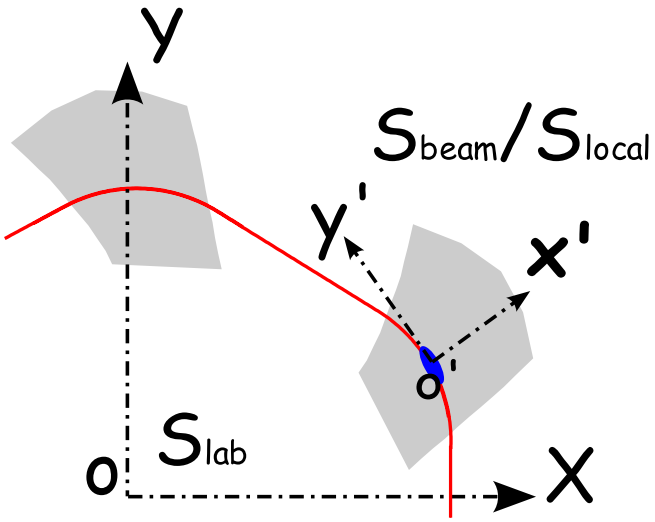

FIG. 2. (Color) Schematic plot of the top view of the three coordinates frames. The red curve is the orbit of bunch center, the blue area represents bunch shape, and the gray area is the hill region of the magnetic field.

At each time step, in order to seek a solution for the space-charge fields, the frames $\mathbf{S}_{\text{local}}$ and $\mathbf{S}_{\text{beam}}$ are redefined according to current 6D phase space distribution, and all particles are transformed from $\mathbf{S}_{\text{lab}}$ to $\mathbf{S}_{\text{local}}$, then a Lorentz transformation is performed to transform all particles to $\mathbf{S}_{\text{beam}}$. The Poisson equation is then solved in the frame $\mathbf{S}_{\text{beam}}$. In a 3D Cartesian frame, the solution of the Poisson equation at point (x, y, z) can be expressed by

$$\phi(x, y, z) = \frac{1}{4\pi\varepsilon_0} \times \int G(x, x', y, y', z, z')\rho(x', y', z')dx'dy'dz', \tag{7}$$

with G the 3D Green function

$$G(x, x', y, y', z, z') = \frac{1}{\sqrt{(x - x')^2 + (y - y')^2 + (z - z')^2}}, \tag{8}$$

assuming open boundary conditions. The typical steps of calculating space-charge fields using the Hockney's fast-Fourier-transform (FFT) algorithm [13] is sketched in Algorithm 1, where the quantities with superscript D (discrete) refer to grid quantities.

With respect to the external magnetic field, two possible situations can be considered: in the first situation, the real field map is available on the median plane of the existing cyclotron machine using measurement equipment. In most cases concerning cyclotrons, the vertical field, B_z, is measured on the median plane ($z = 0$) only. Since the magnetic field outside the median plane is required to compute

Algorithm 1. 3D space-charge calculation

1: **procedure** 3DSpaceCharge (In: ρ, G, Out: $\mathbf{E}_{\rm sc}$, $\mathbf{B}_{\rm sc}$)
2: Create 3D rectangular grid which contains all particles
3: Interpolate the charge q of each macroparticle to nearby mesh points to obtain ρ^D
4: Lorentz transformation to obtain ρ^D in the beam rest frame $\mathbf{S}_{\rm beam}$
5: FFT ρ^D and G^D to obtain $\hat{\rho}^D$ and $\hat{G}^D$
6: Determine $\hat{\phi}^D$ on the grid using $\hat{\phi}^D = \hat{\rho}^D \cdot \hat{G}^D$
7: Use FFT^{-1} of $\hat{\phi}^D$ to obtain ϕ^D
8: Compute $\mathbf{E}^D = -\nabla\phi^D$
9: Interpolate $\mathbf{E}$ at the particle positions $\mathbf{x}$ from $\mathbf{E}^D$
10: Inverse Lorentz transform to obtain $\mathbf{E}_{\rm sc}$ and $\mathbf{B}_{\rm sc}$ in frame $\mathbf{S}_{\rm local}$ and transform back to $\mathbf{S}_{\rm lab}$
11: **end procedure**

trajectories with $z \neq 0$, the field needs to be expanded in the Z direction. According to the approach given by Gordon and Taivassalo [20], by using a magnetic potential and measured B_z on the median plane at the point (r, θ, z) in cylindrical polar coordinates, the 3rd order field can be written as

$$\begin{aligned} B_r(r,\theta,z) &= z\frac{\partial B_z}{\partial r} - \frac{1}{6}z^3 C_r, \\ B_\theta(r,\theta,z) &= \frac{z}{r}\frac{\partial B_z}{\partial \theta} - \frac{1}{6}\frac{z^3}{r}C_\theta, \\ B_z(r,\theta,z) &= B_z - \frac{1}{2}z^2 C_z, \end{aligned} \tag{9}$$

where $B_z \equiv B_z(r,\theta,0)$ and

$$\begin{aligned} C_r &= \frac{\partial^3 B_z}{\partial r^3} + \frac{1}{r}\frac{\partial^2 B_z}{\partial r^2} - \frac{1}{r^2}\frac{\partial B_z}{\partial r} + \frac{1}{r^2}\frac{\partial^3 B_z}{\partial r \partial \theta^2} - 2\frac{1}{r^3}\frac{\partial^2 B_z}{\partial \theta^2}, \\ C_\theta &= \frac{1}{r}\frac{\partial^2 B_z}{\partial r \partial \theta} + \frac{\partial^3 B_z}{\partial r^2 \partial \theta} + \frac{1}{r^2}\frac{\partial^3 B_z}{\partial \theta^3}, \\ C_z &= \frac{1}{r}\frac{\partial B_z}{\partial r} + \frac{\partial^2 B_z}{\partial r^2} + \frac{1}{r^2}\frac{\partial^2 B_z}{\partial \theta^2}. \end{aligned} \tag{10}$$

All the partial differential coefficients are computed on the median plane data by interpolation, using Lagrange's five-point formula.

In the other situation, the 3D field for the region of interest is calculated numerically by building a 3D model using commercial software during the design phase of a new cyclotron. In this case the calculated field will be more accurate, especially at large distances from the median plane, i.e., a full 3D field map can be calculated. For all calculations in this paper, we use the method by Gordon and Taivassalo [20].

Finally, both the external fields and space-charge fields are used to track particles for one time step using a 4th order Runge-Kutta integrator, in which the fields are evaluated for 4 times in each time step. Space-charge fields are assumed to be constant during one time step, because their variation is typically much slower than that of external fields.

B. Neighboring bunch effects

The code is intended to model steady state conditions for the multibunch beam dynamics. In cyclotrons the pattern of turn separation ΔR is affected by many factors. These include machine characteristics such as the magnetic field, the acceleration voltage profile, the accelerating phase of the rf resonators, and initial centering conditions of the injected bunches. Generally, in cyclotrons, ΔR reduces gradually with increasing beam energy. For machines like the PSI injector II, ΔR stays sufficiently large from injection to extraction, and in such cases, neighboring bunch effects are negligible. For others, like the PSI 590 MeV ring cyclotron under consideration in this section, ΔR decreases strongly during the course of acceleration, which results in the need for considering the neighboring bunch effects in order to obtain a precise description of the beam dynamics. In our model, we apply an iterative procedure to determine the number of bunches necessary for a converged simulation. Initially a single bunch with phase space density f_0 and the average radial position R_s is injected. This single bunch is tracked with space charge for one revolution period T_r. Then the new average radial position of the bunch R_e and the bunch rms size $r_{\rm rms} = \sqrt{x_{\rm rms}^2 + y_{\rm rms}^2}$ are calculated from the actual particle distribution. The turn separation ΔR at injection position is then given by $\Delta R = R_e - R_s$. If the condition

$$\Delta R \leq M \times r_{\rm rms} \tag{11}$$

is fulfilled (where M is a parameter given by the user), the 6D phase space is stored as f_{R_e}. The code is switched to multibunch mode, and f_{R_e} will be used as the initial phase space for the following $(N_B - 1)$ neighboring bunches which will be injected one by one per T_r time, where N_B is the number of neighboring bunches given by the user.

If the condition of Eq. (11) is not fulfilled, the value of R_e is assigned to the variable R_s. This single bunch is

Algorithm 2. Multibunch injection algorithm.

1: **procedure** Injection(In: N_B, M, f_0, R_s)
2: Inject f_0 at radius R_s, total bunch number $i_{NB} = 1$
3: Track f_0 for one revolution period T_r, obtain f_{R_e}
4: Calculate radius R_e and bunch size r_{rms}
5: **while** $(R_e - R_s > M \times r_{\mathrm{rms}})$ **do**
6: Save $R_e \rightarrow R_s$
7: Track f_{R_e} for T_r, recalculate R_e and r_{rms}
8: **end while**
9: Save f_{R_e}
10: **while** $(i_{NB} < N_B)$ **do**
11: Inject f_{R_e} and increment i_{NB}
12: Track all bunches for T_r
13: **end while**
14: **end procedure**

tracked with space charge for another revolution period T_r, and the new average radial position of the bunch R_e, the bunch rms size r_{rms}, and the turn separation ΔR are calculated again. After that, the condition in Eq. (11) is evaluated and the same procedure is repeated accordingly.

The underlying assumption for this Ansatz is that all bunches have the same phase space distribution when they reach a certain position, i.e., when f_{R_e} is saved. This is realistic and reasonable when the machine is running in a steady state. It needs to be mentioned that up to that position the coherent instabilities which might be caused by neighboring bunch effects are not covered by this model.

This procedure is summarized in Algorithm 2.

In the multibunch algorithm above, two parameters M and N_B are introduced to set the time of injecting new bunches and the total bunch number, respectively. The proper settings of these two parameters are crucial for the precise evaluation of neighboring bunches effects.

In order to quantify the range of the two parameter N_B and M, let us consider a 2D nonrelativistic DC beam. The Bassetti-Erskine [21] formula for the electric field of a 2D Gaussian charge distribution is in general an analytical expression in terms of the complex error function. In the case of an axisymmetric and Gaussian charge distribution, the electric field can be expressed by

$$\mathbf{E}_{\mathrm{sc}}(r) = \frac{I_0}{2\pi\varepsilon_0\beta c r}\begin{cases}\frac{1-e^{-(r^2/2\sigma^2)}}{1-e^{-(a^2/2\sigma^2)}}\mathbf{n}_r, & r \le a \\ \mathbf{n}_r, & r > a.\end{cases} \tag{12}$$

In this expression, a is the truncated radius, I_0 the beam current, and $\mathbf{n}_r$ the unit vector in the radial direction. Using Eq. (12), it is easy to calculate the electrostatic field generated by N_B Gaussian beams (with N_B an odd number) which are all on a straight line. We can now study the effect of N_B and M on the center beam $N_{Bc} = (N_B + 1)/2$ of the configuration as shown for several configurations in Fig. 3.

Although in the cyclotron the situation is much more complex (the charge distribution and radial position of the bunches are time dependent quantities), we use this model to obtain approximate initial conditions for N_B and M and hence can estimate the contributions for bunches away from N_{Bc}.

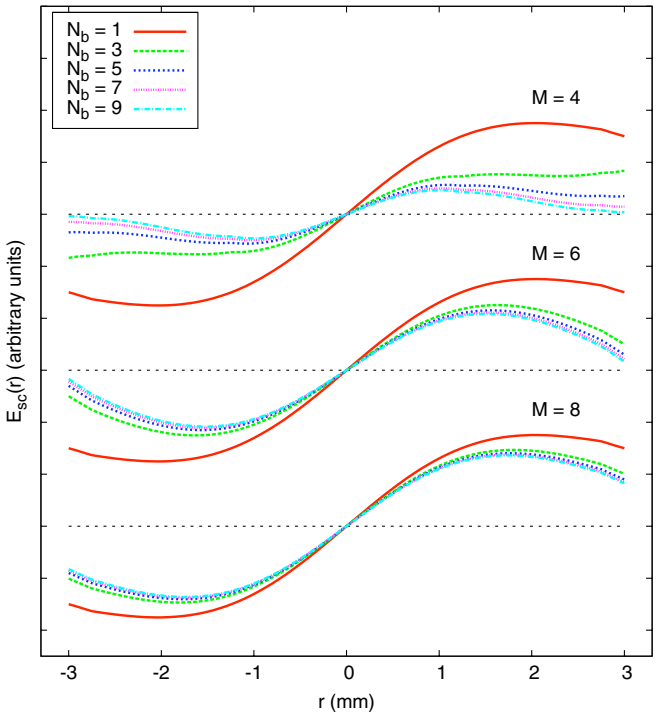

FIG. 3. (Color) The radial space-charge field $E_{\mathrm{sc}}(r)$ of the multiple Gaussian beams at the central beam region. The beams are truncated at 10% of their charge density and rms beam size is $r_{\mathrm{rms}} = 1.0$ (mm). All graphs are on the same scale.

For instance, the setting with $N_B = 9$ and $M = 4.5$ gives convergent results for the PSI ring cyclotron with 3 mA beam current.

In theory, when the maximum bunch number N_B equals the total turn number of the machine, one can eventually obtain the fully self-consistent solution of the problem within our model. In reality, it is not feasible to simulate a full set of bunches, which typically range from several tens to several hundreds. The scale of the number of particles and the dimensions of the needed grid are still beyond the capability of today's supercomputer resources.

In a multibunch simulation the energy of the bunches at different turns can be substantially different. For a multibunch simulation with nine neighboring bunches, if the kinetic energy of the first bunch is $E_k = 100$ MeV and energy gain per turn is $\Delta E_k = 2$ MeV; hence, the velocity difference of the first and last bunch is 6.5%. In this case there is no single rest frame in which the relative motions of particles are nonrelativistic, as required by our scheme to calculate the space-charge forces. Consequently, it is not sufficient to use only one rest frame and one single Lorentz transformation. In order to calculate the space-charge fields more precisely, we use an adaptive binning technique

outlined in Ref. [22] (Sec. V). We note that in our application neither radiation nor retardation effects play a significant role and can therefore be neglected. In the rest frame of the beam, transverse current effects can also be neglected and hence no longitudinal magnetic field component must be considered.

First we create the same amount of energy bins (N_B) as we have bunches in the simulation. An average relativistic factor $\bar{\gamma}_i$ for the ith bunch with N_p^i simulation particles is computed,

$$\bar{\gamma}_i = \frac{\sum_{j=1}^{N_p^i} \sqrt{1 + p_{j,x}^2 + p_{j,y}^2 + p_{j,z}^2}}{N_p^i}, \qquad i = 1 \ldots N_B. \tag{13}$$

Then every particle is grouped into the energy bin whose $\bar{\gamma}_i$ is closest to its γ. In this way, the energy spread of each bin is small and the relative motions of the particles in the same bin are small. After binning we perform the Lorentz transformation, calculate the space-charge field, and perform back-transformation for each bin, respectively. Finally, the field data is summed up to give the total space-charge force imposed on each particle.

The energy spread of the bunches can be large (MeV range), especially in cyclotrons without flattop cavities, and at large radii. This may result in an overlap of energy distributions of neighboring bunches, and hence the energy bins have to be recalculated, i.e., all particles need to be regrouped after each revolution. It is worth noting that, in cyclotrons, the energy difference of neighboring bunches changes with the increasing radius. Therefore the energy difference of the neighboring bins is not constant. Specifically, the energy difference between the ith and $(i-1)$th bins, $\Delta\bar{E}_{i,i-1}$, differs with the energy difference between the $(i+1)$th and the ith bins $\Delta\bar{E}_{i+1,i}$.

III. IMPLEMENTATION WITHIN THE OPAL FRAMEWORK

The above model and algorithm are implemented in the object-oriented parallel PIC code OPAL-CYCL. OPAL-CYCL is one of the flavors of the OPAL (Object-Oriented Parallel Accelerator Library) framework [23]. This framework is a powerful tool for charged-particle optics in general accelerator structures and beam lines using the MAD languages with extensions. OPAL is based on the CLASSIC [24] library and the IP^{2}L framework [25]. The CLASSIC library is a C++ class library which provides services for building portable accelerator models and algorithms and inputting language to specify complicated accelerator systems in general. IP^{2}L is an object-oriented C++ class library which provides abstractions for particles and structured field calculation in a data-parallel programming style. It provides an integrated, layered system of objects. The upper layers contain global data objects of physical/mathematical quantities, such as particles, fields, and matrices of meshes and typical methods performed on these objects such as differential operators and multidimensional FFT's. The lower layers contain the objects relevant to parallelization such as data distribution, domain decomposition, communication among processors, load balancing, and expression templates. Statistical data, such as root mean square (rms) quantities, are computed on the fly (*in situ*) and stored in conjunction with phase space and field data in the H5PART [26] file format. In a postprocessing step, the data can be analyzed using the visualization tool H5PARTROOT [27].

In addition, apart from the multiparticle simulation mode, OPAL-CYCL also has two other serial tracking modes for conventional cyclotron machine design. One mode is the single particle tracking mode, which is a useful tool for the preliminary design of a new cyclotron. It allows one to compute basic parameters, such as reference orbit, phase shift history, stable region, and matching phase ellipse. The other one is the tune calculation mode, which can be used to compute the betatron oscillation frequency ν_r and ν_z. This is useful for evaluating the focusing characteristics of a given magnetic field map.

A more detailed description of the hierarchical layout, the parallelization, and the implementation issues of the OPAL framework and OPAL-CYCL code can be found in the User's Reference Guide [23].

IV. PERFORMANCE TEST AND VALIDATION

In order to evaluate the performance and to benchmark the functionalities of the newly developed code, we performed different types of simulations on the 72 MeV injector II cyclotron of PSI, which has been intensively studied before. Some results are presented in this section.

A. Single particle tracking and tune calculation

In theory, there is an eigenellipse for any given energy in a cyclotron under stable conditions. When the initial phase space matches this eigenellipse, the oscillation of the beam envelope amplitude will be minimal and the transmission efficiency will be maximal. In the present test, the eigenellipse at 2 MeV kinetic energy is calculated using the single particle tracking mode of OPAL-CYCL. The result is compared to FIXPO [28,29]. At PSI the FIXPO code has been the standard simulation tool for the design and parameter optimization of the injector II and the ring cyclotron as well as for a gas driven muon trap in a cyclotron shaped magnetic field. The code integrates single particle orbits by use of a predictor corrector algorithm up to the third order. In Fig. 4 the matched radial ellipse with an initial offset of $x = 2.0$ mm, $p_x = 0.0$ mrad at the symmetry line of the sector field is shown. Excellent agreement is obtained when the time step is set to 1 ps in OPAL-CYCL, although FIXPO uses a different tracking algorithm with the azimuthal angle as the independent variable.

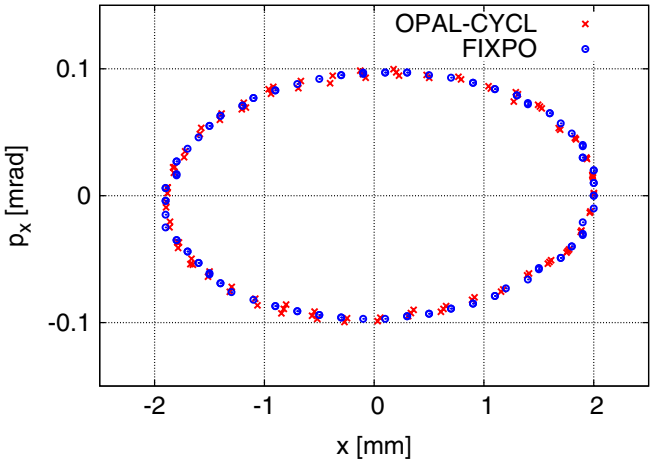

FIG. 4. (Color) Radial eigenellipse of 2 MeV at the symmetric line of a magnet in the injector II cyclotron.

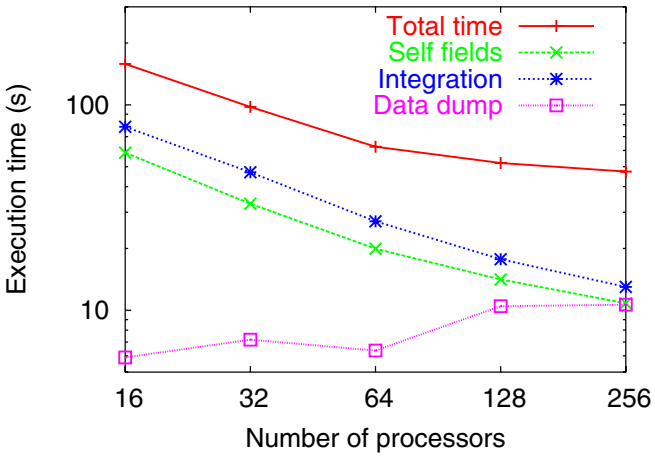

FIG. 6. (Color) The time consumption as a function of processors on Cray XT3, CSCS.

The tune diagram of injector II is computed using the tune calculation mode of OPAL-CYCL, as shown in Fig. 5. The result from FIXPO and OPAL-CYCL are again in good agreement even though different numerical algorithms are used.

The field interpolation scheme, particle tracking, and tuning calculation functionalities are validated substantially by the above tests.

B. Parallel scalability test

In order to observe the parallel scalability of the code, we have performed a detailed study of strong scaling, i.e., the problem size remains constant while increasing the number of computing resources. One million particles are used and tracked 200 time steps on the injector II. The initial beam has a Gaussian-type distribution. The grid size is $64 \times 64 \times 64$ which is decomposed onto a two-dimensional grid of processors. All the intermediate phase space data is dumped into a single H5PART file. The dynamic load balancing frequency as well as the phase space dumping frequency are set to 10. The results are shown in Fig. 6.

We can see that good scalability is achieved up to 128 processors. Above 128 processors, the time consumption of the phase space dumping starts to become significant. The reason for the behavior is the increasing overhead in communication with respect to the amount of data to be stored. Nevertheless, the scalability of the space-charge solver and the particles integrator still benefit from a large number of processors.

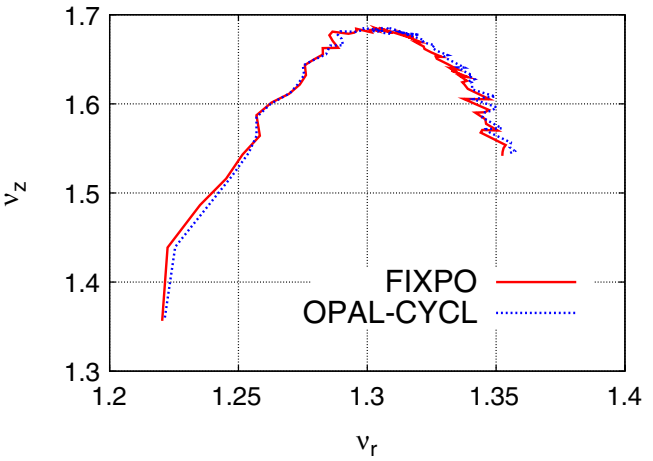

FIG. 5. (Color) Tune diagram of injector II cyclotron, compared with FIXPO code.

C. Stationary round distribution in the PSI injector II

Space-charge effects usually result in an increase in beam size and emittance. That is detrimental to beam dynamics. However, there are cases where space-charge effects can actually play a positive role. The PSI injector II cyclotron is a space-charge dominated machine, in which a very compact stable beam is developed within the first several turns and, thereafter, the charge distribution does not change significantly. This stationary situation remains essentially unchanged until extraction and the beam phase width is about 2° in the last turn. This is due to the combined effect of the strong coupling between the radial and longitudinal directions in the cyclotron and the space charge when the beam current increases above 1 mA. Koscielniak and Adam reproduced this phenomenon by using the serial two-dimensional code PICN [4]. PICN is based on the Needle model, which treats the beam as an ensemble of charged vertical needles with the same height as the beam. In this model, the vertical motion of particles is separated from the horizontal component and the internal motion within needles is neglected. In order to validate the space-charge solver module of our code, we performed the 1 mA, 3 MeV coasting beam simulation on this machine and compared the result with PICN.

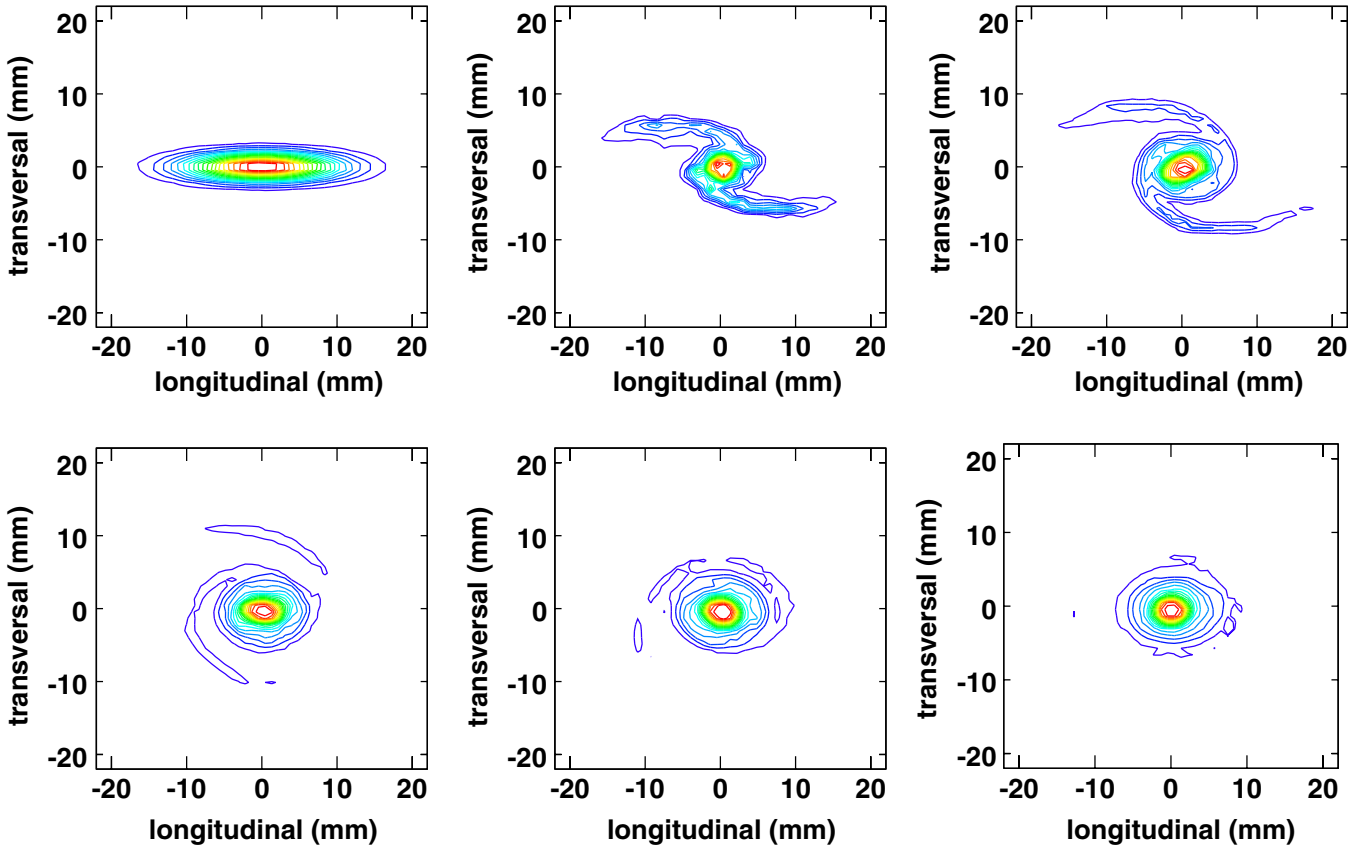

FIG. 7. (Color) Top view of a 1 mA, 3 MeV coasting beam in PSI injector II in the local frame $\mathbf{S}_{\text{local}}$ of PSI injector II. Up: turn 0, 5, 10. Down: turn 20, 30, 40. To compare with figures in Ref. [30], the beam's transport direction is along the negative direction of the abscissa axis.

We used the same initial distribution as in Ref. [30]: $2\sigma_{\text{longitudinal}} = 13.4$ mm (15° phase width), $2\sigma_{\text{transverse}} = 2.52$ mm. The initial emittances of the radial and azimuthal directions are set to zero. In the vertical direction, $2\sigma_z = 4$ mm and $2\sigma_{p_z} = 3.68$ mrad. The total macroparticles number is 1×10^6. Figure 7 shows the top view of beam shape in the local beam frame. We can see that a stable core is developed after about 10 turns, which is faster than the formation of stable haloes.

When comparing Fig. 7 with Fig. 3 and Fig. 4 in Ref. [30] calculated by PICN, we can find the results agree with each other qualitatively. Both of these two codes predict the formation of a compact stable core and wide haloes after 40 turns. However, there still exist visible differences. PICN shows an almost "round" charge density distribution, in the case of OPAL-CYCL we still see low density halo. The longitudinal size of the core is about 2 mm longer than the transverse size. This difference mainly comes from different physical models used in the two codes. PICN uses a so-called smooth approximation which treats the particle orbits as pure circles, but with a sinusoidal radial/vertical focusing (betatron oscillation) having a realistic value of about 1.14 at 3 MeV. Of course, no realistic magnetic field can be azimuthally constant and in the same time focusing in both directions [31]. In addition, all particles in close proximity to the horizontal plane are represented by a single "needle"; in OPAL-CYCL only those particles close to each other in configuration space are represented by a single macroparticle. The latter is believed to be more realistic and accurate.

It can be concluded from this comparison that OPAL-CYCL can reliably reproduce the stable round beam formation caused by space-charge effects in injector II and, hence, can accurately reproduce the single bunch dynamics in cyclotrons.

V. APPLICATIONS

We start this section by describing the two cyclotrons under consideration. The key parameters of the machines are given in Table I. In addition we mention the fundamental rf frequency is 50.633 MHz. In the injector II due to the circular bunch formation, discussed in Sec. IV, the original designed third harmonic flattop resonator is now being used as an additional accelerating structure. It is now obvious to ask the question if one can find a feasible working point for the ring cyclotron with the same characteristics as obtained in the injector II. However, because

TABLE I. Key parameters of the two sector cyclotrons.

	Orbit radius (m)	Kinetic energy (MeV)	Average power (MW)	Average field (T)	Peak field (T)	Magnetic rigidity (Tm)	Harmonic number	Cavity number
Injector II	0.44–3.3	0.87–72	0.15	0.33–0.36	1.08	1.25	10	4
Ring cyclotron	2.1–4.45	72–592	1.3	0.6–0.9	2.17	4.0	6	4 (1 flattop)

of the overlapping turns in the ring cyclotron, the situation is much more complex than in the injector II. Those two issues are addressed for the first time in the remainder of this paper.

A. Different phase width studies of the PSI ring cyclotron

Although a very compact beam with a phase width of about 2° can be extracted from the injector II, it is nevertheless subject to the expansion in the longitudinal direction in the 72 MeV beam transfer line because of space-charge effects and chromatic dispersion. For the future 3 mA beam, this will have a significant impact on the beam dynamic of the ring cyclotron. In response to this, a rebuncher running on the 10th harmonic is planned to be installed on the beam line to make bunches as short as possible at the injection point of the ring cyclotron. The final bunch length achieved is a critical aspect of the ring cyclotron.

In order to obtain a clear perspective on this issue, OPAL-CYCL was applied to do numerical simulation by tracking Gaussian-type beams with three different initial conditions. The initial longitudinal phase widths (6σ) are set to 2°, 6°, and 10°, respectively, and the initial energy spread is neglected. The initial conditions of the horizontal and vertical directions are identical. The initial distribution is not correlated in phase space. The simulation used 10^6 macroparticles and $32 \times 32 \times 32$ grid sizes. The peak voltage of the four main resonators and the 3rd harmonic flattop resonator are 0.9 and 0.403 MV (11.2% of accelerating voltage), respectively. The time step is set to 0.1 ns. It takes about 7 hours on CRAY XT3 of CSCS using 64 processors to track particles from the injection to the extraction.

Figure 8 shows the development of the beam rms size on the transverse and the longitudinal direction. We can see the beam is compressed gradually in the longitudinal direction. Meanwhile, in the transverse direction, the beam size increases fast during the first several turns because of the mismatch of initial conditions. Thereafter, the beam size does not change significantly until the beam arrives at the extraction region where it is distorted by the external magnetic field (extraction bump). Figure 9 shows the projection of phase space onto the midplane of the machine, and Fig. 10 plots the histogram along the longitudinal direction at the 112° azimuthal position of turn 0, 50, and 150. We can see for the bunch with the initial phase width of 2°, the bunch maintains a very compact shape with a stable round core without haloes. When the initial phase width increases, the size of the core only widens slightly (less than 5 mm), while the spiral tails expand in the longitudinal direction and are unable to develop stable haloes. However, the beam does not expand notably in the radial direction, which means no substantial increase of the beam loss on the extraction septum is expected for bunches with initial phase width less than 10°.

B. Neighboring bunch effects in the PSI ring

As discussed in Sec. I, neighboring bunch effects may have an appreciable influence on beam dynamics in the ring. This can be evaluated by comparing the difference in single bunch and multiple bunch simulations as described in Sec. III. We have run simulations for 3, 5, 7, and 9 bunches and found that the difference between the 7 bunch

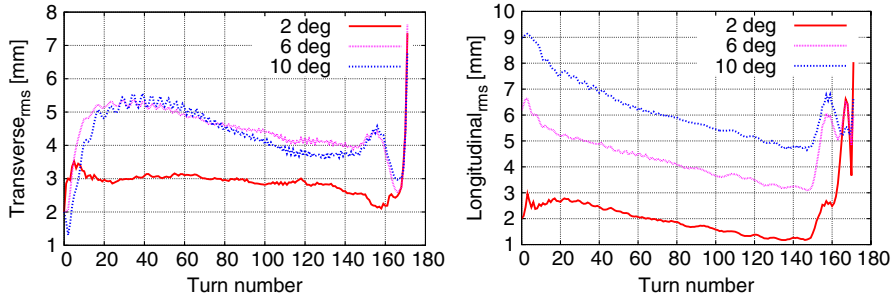

FIG. 8. (Color) Comparison of the rms beam size in the transverse direction (left) and longitudinal direction (right) at the 112° azimuthal position of each turn in the PSI ring cyclotron.

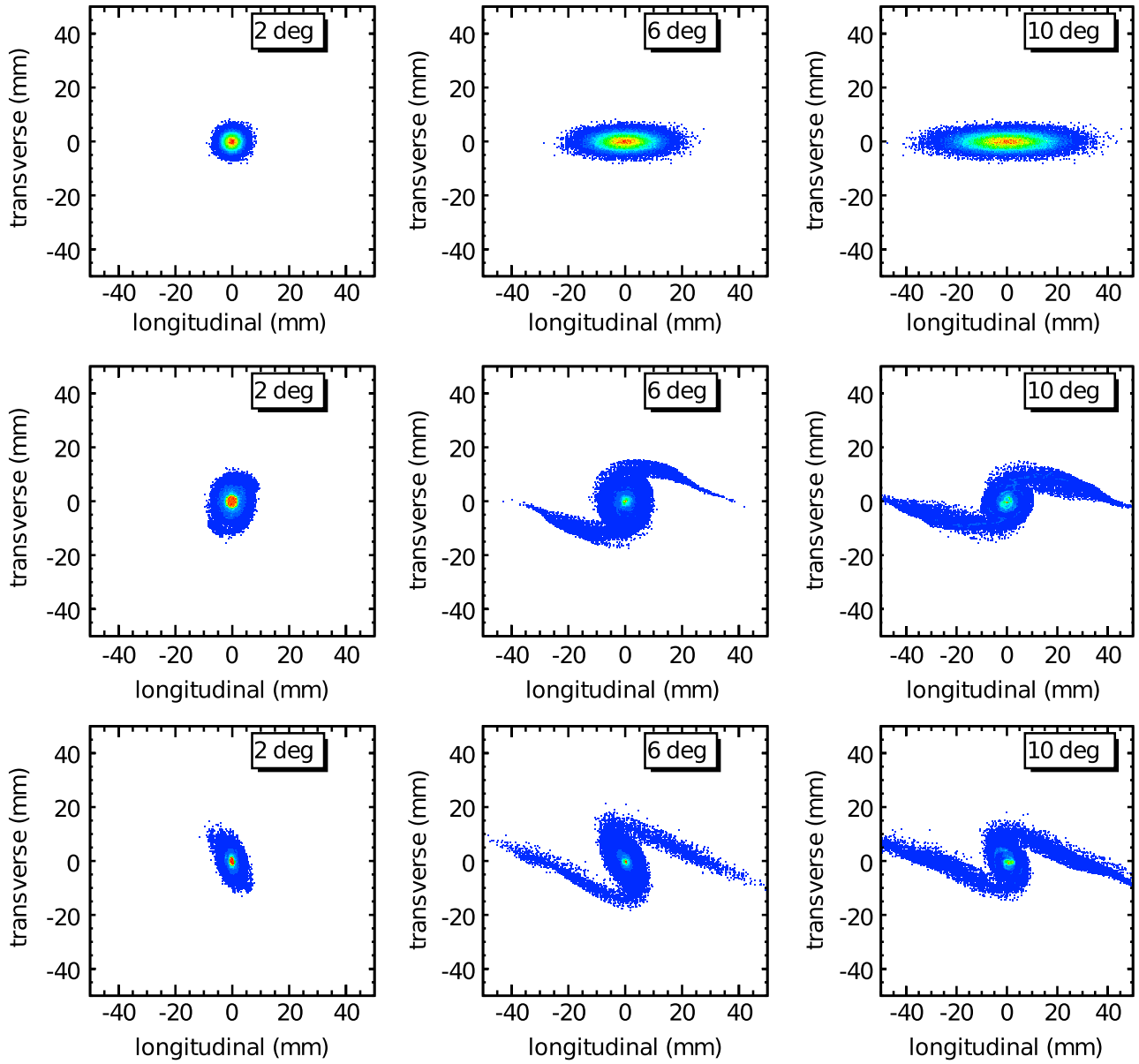

FIG. 9. (Color) Top view of 3 mA bunch distributions with 2°, 6°, and 10° initial phase widths at the initial position (top), turn 50 (middle), and 150 (bottom) in the local frame $\mathbf{S}_{\text{local}}$ of the 112° azimuthal position of the PSI ring cyclotron.

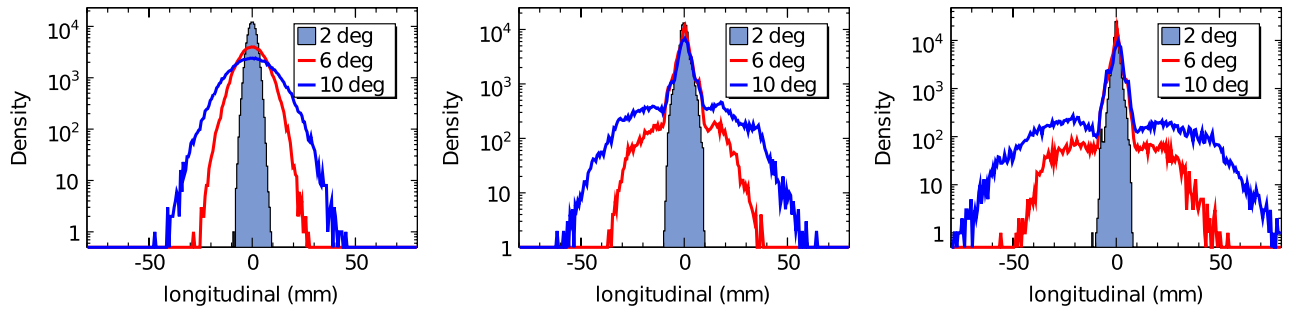

FIG. 10. (Color) Histogram of 3 mA bunch distributions with 2°, 6°, and 10° initial phase widths at initial position (left), turn 50 (middle), and 150 (right) in the PSI ring cyclotron.

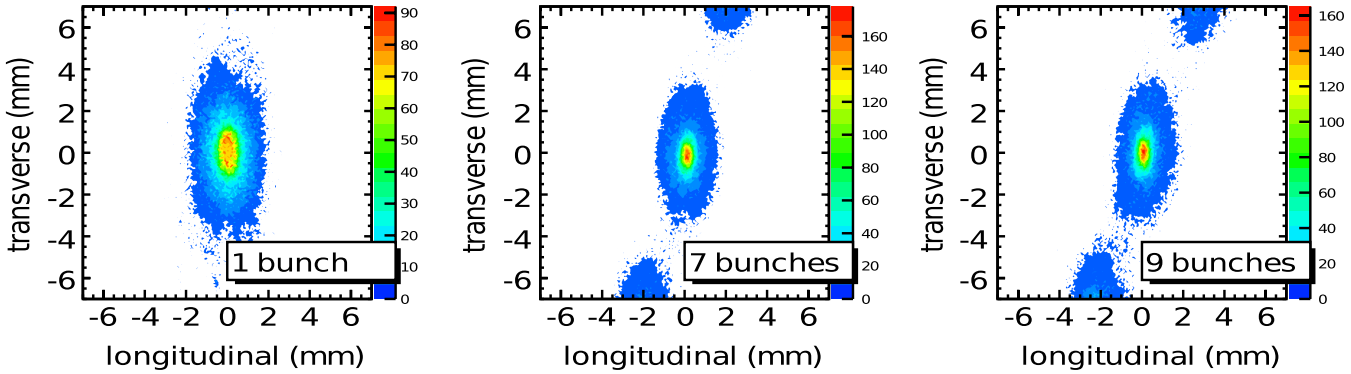

FIG. 11. (Color) Top view of 1 mA bunch distributions at the turn 130 in the local frame $\mathbf{S}_{\text{local}}$ at the 112° azimuthal position of turn 130 in the PSI ring cyclotron. The results are obtained from single bunch (left), seven bunches (middle), and nine bunches (right) simulations, respectively.

scenario and that of 9 bunch scenarios is small, i.e., is viewed as converged, as illustrated in Fig. 11 and discussed already in Sec. II B. From Fig. 12 we conclude that the FWHM of the transverse profile is reduced by approximately 33% comparing a 1 and 9 bunch simulation. For the energy spread (FWHM) we have a reduction in the order of 14%, i.e., from 0.7 to 0.6 MeV.

As Gordon explained in [10], the particle motion in a cyclotron is always perpendicular to the force resulting in a vortex motion. In order to obtain the observed sharpening of the distribution, we need an additional, azimuthal force. A possible explanation of the origin of this force is due to the observed broken circular symmetry when considering neighboring bunches in the simulation. However, more efforts are needed in order to understand this effect in greater detail.

From the comparison, we conclude that the integration of neighboring bunch effects into the model has non-negligible impacts on the beam dynamics for beam currents beyond 1 mA in the PSI ring. The bunch becomes more compact in the transverse direction and the energy spread is slightly reduced. Therefore neighboring bunch effects have a positive influence on reducing beam loss in high intensity operation.

VI. CONCLUSIONS AND DISCUSSIONS

A physical model for the beam dynamics in high intensity cyclotrons, which includes for the first time the space-charge effects of neighboring bunches, is presented in this paper. This model is implemented in an object-oriented three-dimensional parallel PIC code (OPAL-CYCL), as a flavor of the OPAL framework.

The performance tests on the CRAY XT3, CSCS demonstrate a good scalability of OPAL-CYCL with respect to the number of used processors. The three operation modes of this code (tune calculation, single and multiple-particle mode) are validated by code comparison. OPAL-CYCL has been successfully applied to study the behavior of the PSI ring cyclotron at high intensities.

The beam intensity of this high power facility is practically limited by uncontrolled losses at the extraction element of the cyclotron, originating from beam tails that are developed during the acceleration process. As shown in the results, the generation of beam tails can be avoided if short bunches with a phase length of 2° or less are injected. An upgrade plan is under way to generate such short bunches with the help of a 10th harmonic buncher. Furthermore, it is observed that the neighboring bunch effects can help to narrow the transverse beam size and reduce the energy

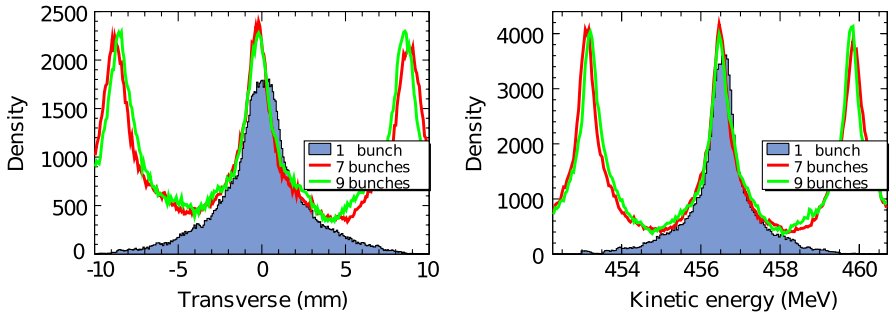

FIG. 12. (Color) Comparison of the histograms along the transversal direction in the local frame $\mathbf{S}_{\text{local}}$ (left) and the energy spectra (right) of 1 mA beam at the 112° azimuthal position of turn 130 in the PSI ring cyclotron.

spread. The differences between single and multibunch simulations are in the order of 33% and 15% in the compared quantities, beam size, and energy spread, respectively. This is a significant difference between single and multibunch simulation, and hence justifies the presented simulation method and their application. This is an important step towards the quantitative understanding of beam tails in high power cyclotrons. Considering the fact that in the PSI ring cyclotron the total sum of controlled and uncontrolled losses are in the order of 10^{-4}, a precise beam dynamics simulation must cover radial neighboring turns in order to predict losses with the mentioned intensities.

It is planned to refine these simulations within the next few years by a more detailed determination of the initial particle distribution at the injection of the PSI ring cyclotron. A quantitative comparison of the results with measured beam quantities will be presented in a future paper.

ACKNOWLEDGMENTS

The authors would like to extend sincere thanks to the Accelerator Modeling and Advanced Computing group members C. Kraus, Y. Ineichen, and B. Oswald for many useful discussions regarding programming and T. Schietinger for providing the postprocessing tool H5PARTROOT. We also feel indebted to W. Joho, S. Adam, and R. Dölling for many helpful discussions regarding high intensity beam dynamics in cyclotrons. This work was performed on the Merlin3 cluster at the Paul Scherrer Institut and on the Cray XT3 at Swiss National Supercomputing Center (CSCS) within the ''Horizon'' collaboration. One author (J. J. Yang) was partially supported by Natural Science Foundation of China (10775185) during his sabbatical at PSI. The authors would also like to thank the referees for a number of suggestions that have substantially improved the form of this work.

[1] R. Baartman, in *Proceedings of the 14th International Conference on Cyclotrons and their Applications* (World Scientific, Capetown, 1995), p. 440.
[2] S. Adam, Ph.D. thesis, ETHZ, Switzerland, 1985, No. 7694.
[3] S. Adam, IEEE Trans. Nucl. Sci. **32**, 2507 (1985).
[4] S. Koscielniak and S. Adam, in *Proceedings of the 15th Particle Accelerator Conference* (IEEE, Washington, DC, 1993), p. 3639.
[5] P. Bertrand and C. Ricaud, in *Proceedings of the 16th International Conference on Cyclotrons and their Applications* (AIP, East Lansing, Michigan, 2001), p. 379.
[6] A. Adelmann, Ph.D. thesis, ETHZ, Switzerland, 2002, No. 14545.
[7] E. Pozdeyev, Ph.D. thesis, MSU, 2003.
[8] M. Humbel (private communication).
[9] W. Kleeven, Ph.D. thesis, TU, Eindhoven, 1988.
[10] M. M. Gordon, in *Proceedings of the 5th International Conference on Cyclotrons and their Applications* (Butterworth, Oxford, 1969), p. 305.
[11] W. Joho, in *Proceedings of the 9th International Conference on Cyclotrons and their Applications* (les Editions de Physique, Caen, 1981), p. 337.
[12] H. Li, Ph.D. thesis, GUCAS, China, 2001.
[13] R. W. Hockney and J. W. Eastwood, *Computer Simulation Using Particles* (Hilger, New York, 1988).
[14] J. Qiang *et al.*, J. Comput. Phys. **163**, 434 (2000).
[15] J. Galambos *et al.*, in *Proceedings of the 18th Particle Accelerator Conference* (IEEE, New York, 1999), p. 3143.
[16] D. Grote *et al.*, Fusion Eng. Des. **32**, 193 (1996).
[17] C. Huang *et al.*, J. Comput. Phys. **217**, 658 (2006).
[18] M. Seidel and P. Schmelzbach, in *Proceedings of the 18th International Conference on Cyclotrons and their Applications* (INFN-LNS, Catania, 2007), p. 157.
[19] T. Zhang, Z. Li, and C. Chu, in Proceedings of the 18th International Conference on Cyclotrons and their Applications (Ref. [18]), p. 33.
[20] M. M. Gordon and V. Taivassalo, IEEE Trans. Nucl. Sci. **32**, 2447 (1985).
[21] M. Bassetti and G. A. Erskine, CERN Technical Report No. CERN-ISR-TH/80-06, 1980.
[22] G. Fubiani, J. Qiang, E. Esarey, and W. P. Leemans, Phys. Rev. ST Accel. Beams **9**, 064402 (2006).
[23] A. Adelmann, C. Kraus, Y. Ineichen, S. Russel, and J. Yang, Paul Scherrer Institut Technical Report No. PSI-PR-08-02, 2008.
[24] F. Iselin, in *Proceedings of the 1996 Computational Accelerator Physics Conference* (AIP, Williamsburg, 1996), p. 99.
[25] A. Adelmann, Paul Scherrer Institut Technical Report No. PSI-PR-09-05, 2009.
[26] A. Adelmann, R. Ryne, J. Shalf, and C. Siegerist, in *Proceedings of the 21st Particle Accelerator Conference* (IEEE, Knoxville, 2005), p. 4129.
[27] T. Schietinger, http://amas.web.psi.ch/tools/H5PartROOT/index.html.
[28] G. Rudolf, FIXPO Bedienungsanleitung, PSI, 2000.
[29] W. Joho, Paul Scherrer Institut Technical Report No. TM-11-07, 1970.
[30] S. Adam, in Proceedings of the 14th International Conference on Cyclotrons and their Applications (Ref. [1]), p. 446.
[31] S. Adam (private communication).